Title
ADVANCED INSTRUMENTATION FOR POSITRON EMISSION TOMOGRAPHY

Authors
Derenzo, S.E.
Budinger, T.F.

Publication Date
1985-04-01

Lawrence Berkeley Laboratory
UNIVERSITY OF CALIFORNIA

Presented at the NATO Advanced Studies Institute Series - Physics and Engineering of Medical Imaging, Maratea, Italy, September 23 - October 5, 1984

ADVANCED INSTRUMENTATION FOR POSITRON EMISSION TOMOGRAPHY

S.E. Derenzo and T.F. Budinger

April 1985

Donner
Biology & Medicine Division

Prepared for the U.S. Department of Energy under Contract DE-AC03-76SF00098

DISCLAIMER

ADVANCED INSTRUMENTATION FOR POSITRON EMISSION TOMOGRAPHY

S.E. Derenzo and T.F. Budinger

Lawrence Berkeley Laboratory
and Donner Laboratory
Berkeley, CA 94720
U.S.A.

ABSTRACT

This paper summarizes the physical processes and medical science goals that underly modern instrumentation design for Positron Emission Tomography. The paper discusses design factors such as detector material, crystal-phototube coupling, shielding geometry, sampling motion, electronics design, time-of-flight, and the interrelationships with quantitative accuracy, spatial resolution, temporal resolution, maximum data rates, and cost.

1 INTRODUCTION

Positron Emission Tomography (PET) serves a unique and important role in medical research because it permits the non-invasive, quantitative study of biological processes as they occur using minute quantities of tracer material. This tracer can be in ionic form, such as 75-second ^{82}Rb, which is rapidly taken up by active heart muscle, or in molecular form, such as 20-min ^{11}C-palmitic acid, which is taken up and oxidized by active heart muscle. Similarly, 108-min ^{18}F-deoxyglucose is taken up by active brain tissue. The physiological processes involved include:

1) Labeled compounds are usually administered by intravenous injection or by inhalation of a radioactive gas. Rapid injections (< 5 sec) are essential when the processes to be studied are also rapid.

2) After passing through the lungs and heart chambers, the tracer is delivered by the arteries to the various tissues in proportion to the blood flow that they receive from the heart. The activity delivered to each organ depends not only on the amount administered, but also on the fraction of cardiac output received and the amount extracted from the lungs during passage of the tracer from the right to the left heart.

3) The tracer is extracted by the tissues through diffusion, active transport or selective binding.

4) The label may undergo several fates, depending on the biochemical processes in the tissue– The tracer may be (i) trapped in its original form, or (ii) diffuse back into the circulation (washout), or (iii) be metabolized and the products either trapped or washed out.

The function of PET instrumentation is the measurement of positron tracer concentration in well-defined volumes as a function of time. Depending on the nature of the tracer and the biochemical processes that it undergoes, compartment models are fit to these data to yield information about tissue extraction, metabolic rate constants, blood volumes, and blood flow. See reference (1) for a review of physiological modeling of PET data.

Section 2 below considers the physical processes that occur during PET and the special advantages of PET for 3-D tomographic imaging.

Section 3 discusses the instrumentation design factors that affect quantitative accuracy, temporal resolution, and spatial resolution.

Section 4 discusses design tradeoffs as well as some recently developed high resolution state-of-the-art tomographs.

2 PHYSICAL CONSIDERATIONS

2.1 PHYSICAL PROCESSES IN PET

The ability of PET instrumentation to measure tracer concentrations is strongly influenced by the physical processes involved in positron emission, the detection of the annihilation photons, and the tomographic reconstruction, which we summarize below in 11 steps:

1) The nucleus decays with the emission of a positron (e^+) and a neutrino (ν). The positrons have a spread of energies from zero to a maximum energy which varies from 0.64 MeV for ^{18}F to 3.35 MeV for ^{82}Rb.

2) The positron looses most of its kinetic energy in the tissue as it travels a few mm from the point of emission to the point of annihilation with a nearby electron (2-4).

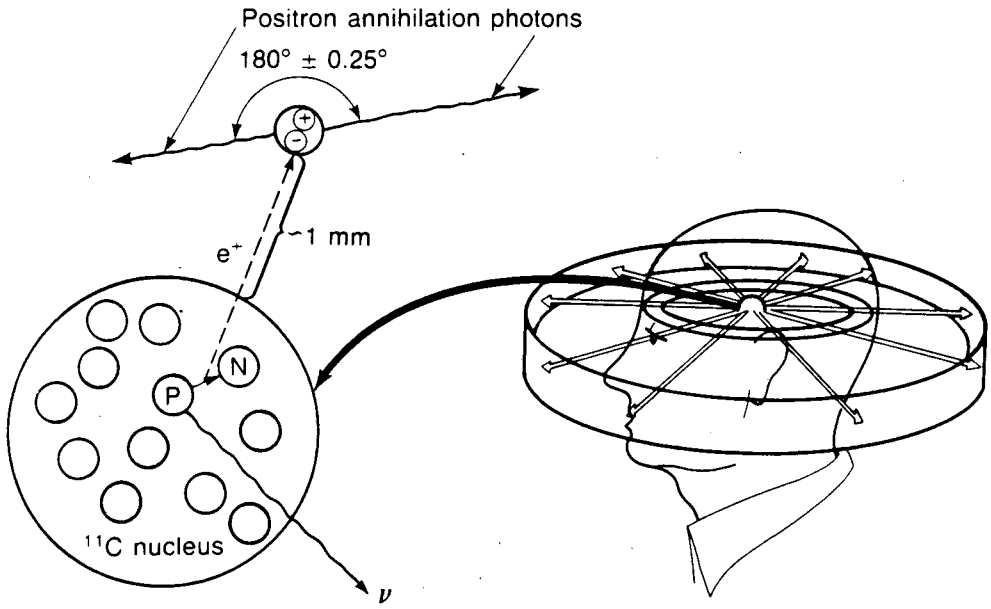

Figure 1: A positron emitted by nuclear decay stops in tissue and annihilates with a nearby electron, producing two 511 keV annihilation photons that fly off in nearly opposite directions.

3) If the positron were able to loose all of its kinetic energy before annihilation, the two 511 keV annihilation photons would be emitted in exactly opposite directions. However, the positron has a residual energy of typically 10 eV, and this causes the angle between the photon pair to have a Gaussian distribution with a full-width at half-maximum (FWHM) of 0.50° (5).

4) A 511 keV photon will travel an average of 10 cm in water before interacting by Compton scattering. This process reduces its energy and randomly changes its direction, effectively loosing all image information. Since the human head or chest is approximately two interaction lengths thick, the probability that both annihilation photons leave the body unscattered is only about 20%. This represents a significant loss of events and requires large correction factors. Also, a small but significant fraction of the annihilation photons scatter "in the plane" of the tomograph and are detected as prompt (non-random) coincidences. These result in a heterogeneous background that extends beyond the subject over the entire imaging field.

5) The annihilation photons can interact in the scintillator in two ways– (i) by photoelectric effect, whereby the entire 511 keV is given to a recoil electron, or (ii) by Compton scattering, where only a portion of the full energy is given to a recoil electron and the photon is reduced in energy and scattered into a new (random) angle. For BGO the probability of a photoelectric event is about 50% for the first interaction. For BaF_2 this probability is about

25%. A successful event requires that both annihilation photons pass the pulse height requirements in both opposing detectors (6,7).

6) The recoil electrons produce ionization and excited atomic electrons in the scintillation crystal. Some of the excited electrons return to their ground states by the emission of scintillation light. The luminous efficiency (number of scintillation photons per keV loss) and the speed of emission vary from crystal to crystal (8).

7) Light in the scintillator can be trapped by total internal reflection, absorbed by internal impurities and imperfections, absorbed by external reflectors, or collected by the photodetector. The collection efficiency is the fraction of light that reaches the photodetector (9).

8) The photodetector converts collected scintillation light to a useful electrical pulse. The quantum efficiency is the probability that an incident photon will produce a photoelectron in the photodetector. The photomultiplier tube has an internal gain of typically 1 million and a single photoelectron produces a pulse several nsec wide and many mV high.

9) Electronic circuits determine whenever two opposing crystals have detected photons within a short time interval (5 to 20 nsec, depending on the detector material) and store the addresses of the crystals involved. For the time-of-flight mode, the differential time of arrival is also recorded.

10) Before tomographic reconstruction, the data must be corrected for (i) the loss of events due to attenuation in the tissue, (ii) accidental background events (random coincident detections of unrelated annihilation photons), (iii) scattered background events (coincident detections of photon pairs from the same positron but one or both have scattered), and (iv) the loss of events due to deadtime in the detectors and electronics.

11) The tomographic reconstruction usually involves filtering the parallel-ray projections either by convolution or frequency filtering and then back-projecting to form the image array. Alternate procedures involve iterative methods of estimating the true distribution such as maximum likelihood or least squares techniques.

Note that 4 different efficiencies appear in these steps:
-detection efficiency (in step 5)
-luminous efficiency (in step 6)
-light collection efficiency (in step 7)
-quantum efficiency (in step 8)

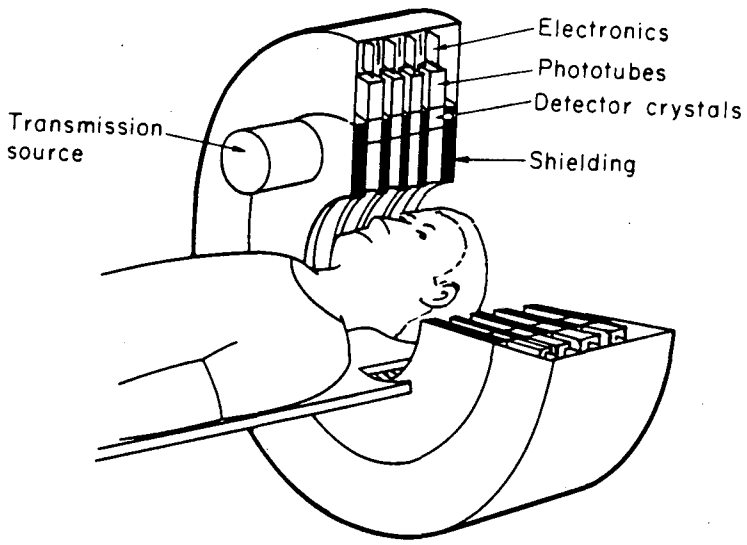

Figure 2: Modern tomograph design using several rings of small crystals that encircle the patient.

2.2 ADVANTAGES OF PET FOR TOMOGRAPHIC IMAGING

Almost all modern positron tomographs use several rings of small crystals that encircle the patient (Figure 2), and utilize the following advantages of PET for tomographic imaging:

1) The total number of coincident events between each detector pair is a measure of all the positron activity along the line between them.

2) The principle of electronic collimation allows small crystals to achieve very good spatial resolution with good sensitivity.

3) The spatial resolution is best at the center of the imaging field, far from material bodies. (In single-gamma imaging, the resolution is best at the front face of the collimator).

4) The sensitivity and spatial resolution are very uniform within the patient port (usually one-half the diameter of the detector ring).

5) Tissue attenuation corrections are straightforward because the attenuation between any two crystals can be measured with an external source and this correction directly applied to the tracer emission data before tomographic reconstruction.

6) Using the difference of arrival time of the coincident photons, the position of the annihilation point along the line between the detector pair can be estimated and this information improves the statistical accuracy (but not the spatial resolution).

Note that PET cannot determine the chemical form of the tracer – metabolic processes must be inferred from the change in measured tracer concentration as a function of time.

3 TOMOGRAPH DESIGN FACTORS

The goal of all tomograph designs is the accurate and rapid measurement of tracer concentration in sharply-defined volume elements in an organ such as the brain or the heart. This requires temporal resolution, spatial resolution, and the quantitative measurement of activity concentration, as discussed below.

3.1 QUANTITATIVE ACCURACY–STATISTICAL FACTORS

Statistical accuracy in the reconstructed image depends on the number of coincident events that can be collected within the available time. This is determined both by the available positron activity and the sensitivity of the tomograph in events per second per radionuclide activity in the imaging field. In addition, some detector materials provide time-of-flight information, which reduces statistical fluctuations in the reconstructed image. The system sensitivity depends on the following 4 factors:

1) Solid angle coverage: Multiple rings of detectors that encircle the patient provide the best acceptance solid angle for the annihilation photons. Utilization of the cross-ring coincidences is very important in realizing the full available solid angle.

2) Axial coverage: Multiple detector rings also serve to cover a larger volume of tissue, thus providing a higher event rate for a given amount of administered tracer activity.

3) Detector Material (Table 1): Except for applications requiring very high light output, BGO has replaced NaI(Tl) in non-time-of-flight PET instrumentation. BGO has the highest density and the highest atomic number of any detector material, and as a result is best able to totally absorb 511 keV photons efficiently in small crystals.

A new material, gadolinium orthosilicate (GSO), was reported in 1982 (10) and has speed advantages over BGO but a lower detection efficiency. Its use is under investigation and is planned for several tomographs (11).

Table 1. DETECTOR MATERIALS FOR PET

Material	NaI(Tl)	CsF	BGO[a]	GSO[b]	BaF_2
Density (gm/cm^3)	3.67	4.61	7.13	6.71	4.8
Atomic Numbers	11,53	55,9	83,32,8	64,16,8	56,9
Emission wavelength (nm)	410	390	480	430	310;225
Index of refraction	1.85	1.48	2.15	1.9	1.56
Hygroscopic	YES	VERY	NO	NO	NO
Photoelectrons per 511 keV	3,000	200	400	600	800;200
Scintillation decay time (nsec)	230	2.5	300	60	620;0.8
Photoelectrons/ns (peak rate)	13	60	1.3	11	1.3;250

[a]bismuth germanate, $Bi_4Ge_3O_{12}$
[b]gadolinium orthosilicate (Cerium activated), $Gd_2SiO_5(Ce)$

BaF_2 has replaced CsF for time-of-flight positron instrumentation. In 1982 a very fast (800 psec) scintillation component was discovered, making BaF_2 the highest speed inorganic scintillator known (12). BaF_2 is not hygroscopic (unlike CsF) and the crystals do not have to be sealed in bulky cans, which improves the detection efficiency.

For any detector material, the detection efficiency depends on the detector material, size, and pulse height thresholds used (6,7).

4) Time-of-flight information: Modern BaF_2 detectors have excellent timing resolution (typically 400 psec FWHM) and are able to measure the arrival time difference between the two photons and determine the annihilation point with an uncertainty of 6 cm FWHM. In conventional tomography, the annihilation point is only known to lie somewhere along the line between the two coincident detectors. The time-of-flight information is able to reduce the rms statistical uncertainty in the reconstructed image by the ratio of the distance across the emitting region to the time-of-flight uncertainty times twice the speed of light (15 cm per nsec) (13-15). For example, for a time-of-flight uncertainty of 6 cm and a 24 cm diam emission region, the time-of-flight information reduces the statistical uncertainty by a factor of 2 which corresponds to a four-fold decrease in the imaging time.

3.2 QUANTITATIVE ACCURACY–SYSTEMATIC FACTORS

PET data are subject to 6 major systematic errors:

1) attenuation of the annihilation photons in the tissue

2) partial volume effects due to limited axial resolution

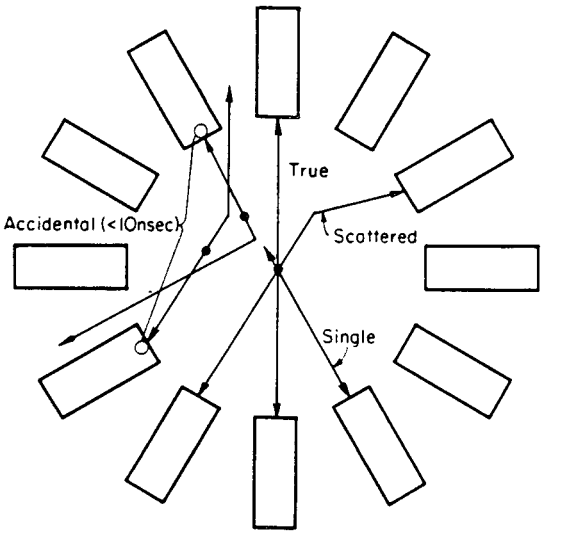

Figure 3: Types of Positron Annihilation Events–
True events are coincident detections of unscattered photon pairs from the same e^+.
Scattered events are coincident detections of photon pairs from the same e^+ where one or both have scattered.
Accidental events are unrelated photons detected in coincidence by chance.

3) smearing due to limited in-plane resolution (16)

4) background events due to accidental coincidences (17,18)

5) background events due to prompt scatter (18-21)

6) losses due to deadtime in the detectors and electronic circuits

The two types of events leading to background types 4) and 5) are illustrated in Figure 3.

3.3 TEMPORAL RESOLUTION

The ability to measure the tracer concentration with good temporal resolution (i.e. in a series of rapid time sequence images) requires the collection of a large number of events during the study, which requires good detection efficiency, low deadtime, high maximum data rates, and a minimum of detector motion. Note the ability to fit compartment model rate constants to PET data depends primarily on the total number of events collected in the study and the temporal resolution. The number of events in each time sequence image is of less importance.

3.4 SPATIAL RESOLUTION

Quantitation within regions of size D requires combined system spatial resolution with FWHM $\leq$ D/2. Eight components of the system resolution are discussed below:

Table 2. POSITRON RANGES IN WATER

Isotope	^{18}F	^{11}C	^{68}Ga	^{82}Rb
Maximum Energy	0.64 MeV	0.96 MeV	1.90 MeV	3.35 MeV
PSF FWHM[a]	0.13 mm	0.13 mm	0.31 mm	0.42 mm
PSF rms[b]	0.23 mm	0.39 mm	1.2 mm	2.6 mm
Diameter(75%)	1.2 mm	2.1 mm	5.4 mm	12.4 mm

[a]Full width at half maximum of projected point spread function
[b]Root-mean-square deviation from center of projected point spread function
[c]Diameter of circle containing 75% of the projected annihilations

1) The positron range distribution is sharply peaked and has narrow FWHM and standard deviation values (Table 2). However, most of the annihilations occur in the extensive tails of the distribution, as evidenced by the diameter of the circle that contains 75% of the projected annihilation points (2-4).

2) The deviations from 180° have a nearly Gaussian distribution with a FWHM of 0.50° (5). This contributes 1.3 mm FWHM for a 60 cm diam detector ring.

3) The geometrical component of the detector resolution (at the center of the imaging port) is approximately equal to one-half of the detector width (22-24).

4) Annihilation photons from off-axis sources can penetrate one or more detectors before interacting and this results in a radial elongation of the PSF at the edge of the field (25,26).

5) Compton scattering of the annihilation photons in the detectors can result in a mis-identification of the detector of first interaction. This can be reduced by (i) coupling each scintillator to its individual photodetector and requiring single detector interactions only (22), or (ii) placing shielding material between the detectors, but this reduces the detection efficiency, especially for off-angle rays (6,23,24).

6) For detectors of width W, the geometrical resolution of W/2 discussed in part 3) above will not be realized in the reconstructed image unless the tomographic sampling distance is W/4 or finer throughout the image region. A stationary circular array has a sampling distance of W/2. The most frequently employed method of improving the sampling is by the "wobble" motion- rotating the detector array about a small circle centered at the system axis (27-30). A sampling distance of W/4 can also be achieved with only two mechanical positions by using the "clam" motion (31).

7) reconstruction filter frequency roll-off should be determined by the system resolution, not by statistical fluctuations

8) the effects of organ and tracer motion are reduced by gating for cardiac imaging and rapid sequence imaging for fast dynamic processes

4 TOMOGRAPH DESIGN FACTORS

4.1 CRYSTAL-PHOTOTUBE COUPLING

One of the most fundamental limits to detector resolution is that available phototubes are larger than the crystals we wish to use. Below we summarize many of the efforts to couple small crystals to larger phototubes:

1) Several groups over the years have coupled phototubes to a larger number of smaller crystals so that the light may be split between several phototubes. The light ratio is then used to identify which crystal is scintillating (32-35).

2) Several positron detectors (starting with the Anger positron camera) use the large light output of NaI(Tl) so that signals from several phototubes coupled to a single large crystal of NaI(Tl) can be used to determine the location of the scintillation point (36,37).

3) In another approach a grid of wires is mounted between one or more scintillation crystals and the photocathode of a photomultiplier tube. After the appearance of a photomultiplier pulse, portions of the grid are selectively pulsed to alter the electron trajectories near the adjacent photocathode. The scintillating crystal can thus be identified because the phototube output pulse will only be affected when the associated portion of the grid is pulsed (38-41).

4) Some effort has been directed toward developing phototubes with multiple electron multipliers and anodes, to eliminate some of the glass walls between phototubes, but this approach is presently limited to crystals 6 mm or larger. (42-45).

5) A most promising recent approach uses a photomultiplier combined with solid state photodetectors. A group of crystals is coupled to a relatively large photomultiplier tube which determines the timing for the group. The solid-state photodetectors are coupled individually to each crystal to determine the identity of the scintillating crystal. HgI_2, (46-48) silicon photodiodes (22,49,50), silicon avalanche photodiodes (51-54), and small low-gain phototubes (41) have been suggested for the crystal identifier.

4.2 TRADEOFFS IN TOMOGRAPH DESIGN

1) Patient port size:- A head tomograph has a smaller patient port than a whole-body tomograph (30 cm vs 50 cm diam) and a smaller detector ring (60 cm vs 100 cm diam). This results in increased sensitivity, lower cost (fewer detectors) and improved spatial resolution because the angulation error is less. The primary advantage of the body tomograph is that it can image the human thorax and abdomen.

2) Shielding gap thickness, S: A large shielding gap enhances the sensitivity because the image event rate varies as S^2. However, increasing S increases the scatter backgrounds (which vary as S^3), and increases the accidental backgrounds (which vary as S^4). For single ring systems, the shielding gap defines the slice thickness. For multiple ring systems, the relationship between axial resolution, sensitivity, and backgrounds is more involved as it depends on the design of the inter-ring shielding.

3) Shielding depth: Given a patient port size and shielding gap thickness, it is possible to select a shielding depth that minimizes the statistical fluctuations in the reconstructed image. A smaller shielding depth reduces the detector diameter and enhances the sensitivity for image-forming events, but also increases the number of scattered and random background events. A greater shielding depth reduces these backgrounds but also reduces the image-forming events. An analysis of these tradeoffs is treated in reference (18).

4) Positron isotopes and compounds: As shown in table 2, some of the positron-emitting isotopes (such as ^{18}F) have less blurring due to positron range and are preferred whenever high spatial resolution is important. Isotopes with a short half life and advantageous biodistribution are also preferred because a large amount of tracer activity can be used for a given radiation dose to the patient, and this provides good counting statistics.

5) Time-of-flight vs conventional tomography : BaF_2 provides very good timing resolution which results in low accidental backgrounds, very high maximum event rates, and information on the location of the point of annihilation which reduces the statistical fluctuations in the reconstructed image. However, this advantage is partially offset by the reduced detection efficiency and a greater difficulty in using small crystals for good spatial resolution. BGO provides the ability to use smaller crystals and phototubes and simplifies the electronics and data storage.

6) Number of detectors: The use of many small detectors aids in reducing the overall system deadtime and in improving spatial resolution. However, the cost of the tomograph is related to the number of detectors.

7) Circuit deadtime: The use of many parallel circuits increases the cost of the electronics but can provide very high data rates, even when using BGO, which is relatively slow.

8) The reconstruction algorithm: By using a reconstruction filter that maintains the higher spatial frequencies (within the limits of the overall system spatial resolution), quantitation within well-defined volume elements is improved. Reducing the amplitude of these higher frequencies decreases the apparent noise in the reconstructed images and is frequently used when the tomographic reconstruction is to be viewed as an image.

9) Sampling motion: The use of a detector sampling motion improves the image quality and quantitation by more densely sampling the image space. However, this motion conflicts with requirements for high temporal resolution, particularly for gated cardiac imaging. Although the most common sampling motion is the circular "wobble", the "clam" motion involves only two positions and can be peformed even for gated cardiac studies.

See references (11,44,55-59) for more complete discussions of these factors in tomograph design.

4.3 ADVANCED TOMOGRAPHS

Table 3 describes some modern positron tomographs with <7 mm resolution.

See references (60-62) for descriptions of positron tomographs using time-of-flight information.

Table 3. COMPARISON OF POSITRON TOMOGRAPHS WITH SPATIAL RESOLUTIONS FINER THAN 7 mm FWHM

Institution References	MGH Boston (63-66)	NIRS Japan (67,68)	CTI Knoxville (69)	LBL Berkeley (70)	Univ Penn (71,72)
Detector Material	BGO	BGO	BGO	BGO	NaI(Tl)
Number of Rings	1	1	1-4	1	1
Number of Crystals	360	128	512[a]	600	6
Detector Ring Diam (cm)	46	26.5	100	60	85[b]
Patient Port Diam (cm)	28	13.5	65	30	50
Crystal Width (mm)	4	4	5.6	3	–
Crystal C-C Spacing (mm)	4.0	6.5	6.1	3.15	–
In-plane Resolution (mm)[c]	4.8	3	5	2.6	6.5
Axial Resolution (mm)	10	5	18	5	13

[a] per ring
[b] hexagonal
[c] FWHM of reconstructed point spread function near center of system

5 CONCLUSIONS

1) Positron Emission Tomography measures regional biochemical processes (and is complementary to X-ray CT and Magnetic Resonance Imaging).

2) The choices of detector material, crystal-photomultiplier coupling, sampling motion, and shielding geometry have a significant effect on spatial resolution, temporal resolution, and the ability to accurately measure tracer concentration.

3) Multilayer tomograph designs are important in being able to collect more information for a given administered activity.

4) PET instrumentation has evolved in two distinct directions: (a) the use of very small BGO or GSO crystals for high spatial resolution (<5mm FWHM) conventional tomography or (b) the use of BaF_2 with good timing resolution (<500 psec FWHM) for time-of-flight tomography.

5) Efforts are underway throughout the world to improve the timing resolution of BGO and GSO systems, and to improve the spatial resolution of BaF_2 systems.

ACKNOWLEDGEMENTS

We thank R. Huesman and J. Cahoon for helpful discussions.

This work was supported in part by the Director, Office of Energy Research, Office of Health and Environmental Research of the U.S. Department of Energy, under Contract No. DE-AC03-76SF00098, and in part by the National Institutes of Health, National Heart, Lung, and Blood Institute under grant No. P01 HL25840.

Reference to a company or product name does not imply approval or recommendation of the product by the University of California or the U.S. Department of Energy to the exclusion of others that may be suitable.

REFERENCES

1. Budinger TF, Huesman RH, Knittel B, Friedland R, and Derenzo SE: Physiological modeling of dynamic measurements of metabolism using positron emission tomography. In *The Metabolism of the Human Brain Studied with Positron Emission Tomography,* T. Greitz, Ed, Raven Press, New York, pp 165-183, 1984

2. Cho ZH, Chan JK, Eriksson L, et al: Positron ranges obtained from biomedically important positron-emitting radionuclides. *J Nucl Med* 16: 1174-1176, 1975

3. Phelps ME, Hoffman EJ, Huang SC, et al: Effect of positron range on spatial resolution. *J Nucl Med* 16: 649-652, 1975

4. Derenzo, SE: Precision measurement of annihilation point spread distributions for medically important positron emitters. In: *Positron Annihilation,* Hasiguti RR and Fujiwara K, eds, pp 819-823, The Japan Institute of Metals, Sendai, Japan, 1979

5. Colombino P, Fiscella B, Trossi L: Study of positronium in water and ice from 22 to -144 °C by annihilation quantum measurements. *Nuovo Cimento* 38: 707-723, 1965

6. Derenzo SE: Monte Carlo calculations of the detection efficiency of arrays of NaI(Tl), BGO, CsF, Ge, and plastic detectors for 511 keV photons. *IEEE Trans Nucl Sci* NS-28: 131-136, 1981

7. Derenzo SE: Comparison of detector materials for time-of-flight positron tomography. *Proceedings of the International Workshop on Time-of-Flight Positron Tomography,* Thomas LJ and Ter-Pogossian MM, eds. pp 63-68, IEEE Computer Society Cat No 82CH1791-3, 1982.

8. Birks JB: *The Theory and Practice of Scintillation Counting* Pergamon Press, Oxford, England, 1964, pp 473-474

9. Derenzo SE and Riles J: Monte Carlo calculations of the optical coupling between bismuth germanate crystals and photomultiplier tubes. *IEEE Trans Nucl Sci* NS-29: 191-195, 1982

10. Takagi K, and Fukazawa T: Cerium activated Gd_2SiO_5 single crystal scintillator. *Appl Phys Lett* 42: 43-45, 1983

11. Eriksson L, Bohm C, Kesselberg M, et al: A high resolution positron camera. In *The Metabolism of the Human Brain Studied with Positron Emission Tomography,* Greitz T, ed, Raven Press, New York, 1985, pp 13-20

12. Gariod R, Allemand R, Cormoreche E, et al: The LETI positron tomograph architecture and time of flight improvements. *Workshop on Time-of-Flight Tomography,* IEEE Catalog No 82CH1719-3, 1982.

13. Snyder DL, Thomas LJ and Ter-Pogossian MM: A mathematical model for positron-emission tomography systems having time-of-flight measurements. *IEEE Trans Nucl Sci* NS-28: 3575-3583, 1981

14. Tomitani T and Tanaka E: Image reconstruction and noise evaluation in photon time-of-flight assisted positron emission tomography. *IEEE Trans Nucl Sci* NS-28: 4582-4589, 1981

15. Snyder DL: Some noise comparisons of data-collection arrays for emission tomography-systems having time-of-flight measurements. *IEEE Trans Nucl Sci* NS-29: 1029-1033, 1982

16. Hoffman EJ, Huang SC, and Phelps ME: Quantitation in positron emission tomography: 1. Effect of object size. *J Comput Assist Tomogr* 3: 299-308, 1979

17. Burnham CA, Alpert NM, Hoop B, Jr., et al: Correction of positron scintigrams for degradation due to random coincidences. *J Nucl Med* 18: 604 (Abstract), 1977

18. Derenzo SE: Method for optimizing side shielding in positron emission tomographs and for comparing detector materials. *J Nucl Med* 21: 971-977, 1980

19. Wong WH and Adler S: Characterization of the scattered radiation fraction in PET or SPECT cameras with a novel phantom design. *IEEE Trans Nucl Sci* NS-32: 831-834, 1985

20. Bergström M, Eriksson L, Bohm C, Blomqvist G and Litton J: Correction for scattered radiation in a ring detector positron camera by integral transformation of the projections. *J Comput Assist Tomogr* 7: 42-50, 1982

21. Bruno MF, Huesman RH, Derenzo SE, and Budinger TF: Characterization of Compton Scattering in Emission Tomography. *J Nucl Med,* 25: P14, 1984

22. Derenzo SE: Initial characterization of a BGO-silicon photodiode detector for high resolution PET. *IEEE Trans Nucl Sci* NS-31(1): 620-626, 1984

23. Holmes TJ and Ficke DC: Analysis of positron-emission tomography scintillation-detectors with wedge faces and inter-crystal septa. *IEEE Trans Nucl Sci* NS-32: 826-830, 1985

24. Kesselberg M, Bohm C, Litton JE, et al: Design considerations of small crystal positron camera systems. *IEEE Trans Nucl Sci* NS-32: 907-911, 1985

25. Derenzo SE, Budinger TF, Cahoon JL, Greenberg WL, Huesman RH, and Vuletich T: The Donner 280-crystal high resolution positron tomograph. *IEEE Trans Nucl Sci* NS-26: 2790-2793, 1979

26. Eriksson L, Bohm C, Kesselberg M, et al: A four ring positron camera system for emission tomography of the brain. *IEEE Trans Nucl Sci* NS-29: 539-543, 1982

27. Bohm C, Eriksson L, Bergström M, et al: A computer assisted ring detector positron camera system for reconstruction tomography of the brain. *IEEE Trans Nucl Sci* NS-25: 624-637, 1978

28. Brooks RA, Sank VJ, Talbert AJ, et al: Sampling requirements and detector motion for positron emission tomography. *IEEE Trans Nucl Sci* NS-26: 2760-2763, 1979

29. Herman GT: The mathematics of wobbling a ring of positron annihilation detectors. *IEEE Trans Nucl Sci* NS-26: 2756-2759, 1979

30. Colsher JG and Muehllehner G: Effects of wobbling motion on image quality in positron tomography. *IEEE Trans Nucl Sci* NS-28: 90-93, 1981

31. Huesman RH, Derenzo SE and Budinger TF: A two-position sampling scheme for positron emission tomography. In *Nuclear Medicine and Biology,* Raynaud C, ed., Pergammon Press, New York, Vol I, pp 542-545, 1983.

32. Burnham CA and Brownell GL: A multi-crystal positron camera. *IEEE Trans Nucl Sci* NS-19(3): 201-205, 1972

33. Burnham C, Bradshaw J, Kaufman D, et al: Application of a one dimensional scintillation camera in a positron tomographic ring detector. *IEEE Trans Nucl Sci* NS-29(1): 461-464, 1982

34. Takami K, Ishimatsu K, Hayashi T, et al: Design considerations for a continuously rotating positron computed tomograph. *IEEE Trans Nucl Sci* NS-29: 534-538, 1982

35. Ricci A, Hoffman E, Phelps M, et al: Investigation of a technique for providing a pseudo-continuous detector ring for positron tomography. *IEEE Trans Nucl Sci* NS-29: 452-456, 1982

36. Anger HO: Survey of radioisotope cameras. *ISA Trans* 5: 311-334, 1966

37. Muehllehner G, Colsher JG, and Lewitt RM: A hexagonal bar positron camera: problems and solutions. *IEEE Trans Nucl Sci* NS-30: 652-660, 1983

38. Charpak G: The localization of the position of light impact on the photocathode of a photomultiplier. *Nucl Instr Meth* 48: 151-153, 1967

39. Charpak G: Retardation effects due to the localized application of electric fields on the photocathode of a photomultiplier. *Nucl Instr Meth* 51: 125-128, 1967

40. Boutot JP and Pietri G: Photomultiplier control by a clamping cross-bar grid. *IEEE Trans Nucl Sci* NS-19(3): 101-106, 1972

41. Yamashita Y, Uchida H, Yamashita T and Hayashi T: Recent development in detectors for high spatial resolution positron CT. *IEEE Trans Nucl Sci* NS-31, 424- 428, 1984

42. Murayama H, Nohara N, Tanaka E, et al: A quad BGO detector and its timing and positioning discrimination for positron computed tomography. *Nucl Instr Meth* 192: 501-511, 1982

43. Uchida H, Yamashita Y, Yamashita T, et al: Advantageous use of new dual rectangular photomultiplier for positron CT. *IEEE Trans Nucl Sci* NS-30: 451-454, 1983

44. Okajima K, Ueda K, Takami K, et al: Performance study of the whole-body, multilayer positron computed tomograph –PCTW–II–. *IEEE Trans Nucl Sci* NS-32: 902-906, 1985

45. Kume H, Suzuki S, Takeuchi J, et al: Newly developed photomultiplier tubes with position sensitivity capability. *IEEE Trans Nucl Sci* NS-32: 448-452, 1985

46. Barton JB, Hoffman EJ, Iwanczyk JS, et al: A high-resolution detection system for positron tomography. *IEEE Trans Nucl Sci* NS-30: 671-675, 1983

47. Groom DE: Silicon photodiode detection of bismuth germanate scintillation light, *Nucl Instr Meth,* 219: 141-148, 1984

48. Iwanczyk JS, Barton JB, Dabrowski AJ, et al: A novel radiation detector consisting of an HgI_2 photodetector coupled to a scintillator. *IEEE Trans Nucl Sci* NS-30: 363-367, 1983

49. Derenzo SE: Gamma-ray spectroscopy using small, cooled bismuth germanate scintillators and silicon photodiodes. *Nucl Instr Meth,* 219: 117-122, 1984

50. Derenzo SE, Budinger TF, and Huesman RH: Detectors for high resolution dynamic PET. In *The Metabolism of the Human Brain Studied with Positron Emission Tomography,* T. Greitz, Ed, Raven Press, New York, pp 21-31, 1984

51. Entine E, Reiff G, Squillante M, et al: Scintillation detectors using large area silicon avalanche photodiodes. *IEEE Trans Nucl Sci* NS-30: 431-435, 1983

52. Lecomte R, Schmitt D, Lightstone AW, et al: Performance characteristics of BGO-silicon avalanche photodetectors for PET. *IEEE Trans Nucl Sci* NS-32: 482-486, 1985

53. Dahlbom M, Mandelkern MA, Hoffman EJ, et al: Hybrid mercuric iodide (HgI_2) – gadolinium orthosilicate (GSO) detector for PET. *IEEE Trans Nucl Sci* NS-32: 533-537, 1985

54. Squillante MR, Reiff G, and Entine G: Recent advances in large area avalanche photodiodes. *IEEE Trans Nucl Sci* NS-32: 563-566

55. Uemura K, Kanno I, Miura S, et al: High resolution positron tomograph: HEADTOME III: system description and preliminary report on the performances. In *The Metabolism of the Human Brain Studied with Positron Emission Tomography*, Greitz T, ed, Raven Press, New York, 1985, pp 47-56

56. Brooks RA, Friauf WS, Sank VJ, et al: Initial evaluation of a high resolution positron emission tomograph. In *The Metabolism of the Human Brain Studied with Positron Emission Tomography*, Greitz T, ed, Raven Press, New York, 1985, pp 57-68

57. Hoffman EJ, van der Stee M, Ricci AR, et al: System features that are determinate in precision and accuracy in positron emission tomographs. In *The Metabolism of the Human Brain Studied with Positron Emission Tomography*, Greitz T, ed, Raven Press, New York, 1985, pp 69-84

58. Brooks RA, Sank VJ, Friauf WS, Leighton SB, Cascio HE and DiChiro G: Design considerations for positron emission tomography. *IEEE Trans Biomed Eng* BME-28: No 2, 158-177, 1981

59. Budinger TF, Derenzo SE, Huesman RH and Cahoon JL: Medical criteria for the design of a dynamic positron tomograph for heart studies. *IEEE Trans Nucl Sci* NS-29: 488-492, 1982

60. Ter-Pogossian MM, Mullani NA, Ficke DC, et al: Photon time-of-flight-assisted positron emission tomography. *J Comput Assist Tomogr* 5: 227-239, 1981

61. Mullani NA, Gaeta J, Yerian K, et al: Dynamic imaging with high resolution time-of-flight PET camera - TOFPET I. *IEEE Trans Nucl Sci* NS-31: 609-613, 1984

62. Soussaline F, Comar D, Allemand R, et al: New developments in positron emission tomography instrumentation using the time-of-flight information. In *The Metabolism of the Human Brain Studied with Positron Emission Tomography*, Greitz T, ed, Raven Press, New York, 1985, pp 1-12

63. Burnham CA, Bradshaw J, Kaufman D, et al: A stationary positron emission ring tomograph using BGO detector and analog readout. *IEEE Trans Nucl Sci* NS-31(1): 632-636, 1984

64. Brownell GL, Burnham CA and Chesler DA: High resolution tomograph using analog coding. In *The Metabolism of the Human Brain Studied with Positron Emission Tomography*, Greitz T, ed, Raven Press, New York, 1985, pp 13-20

65. Stearns CW, Chesler DA, Kirsch JE, et al: Quantitative imaging with the MGH analog ring positron tomograph. *IEEE Trans Nucl Sci* NS-32: 898-901, 1985

66. Burnham CA, Bradshaw J, Kaufman D, et al: Design of cylindrical shaped scintillation camera for positron tomographs. *IEEE Trans Nucl Sci* NS-32: 889-893, 1985

67. Nohara N, Tanaka E, and Tomitani T: Analytical study of performance of high resolution positron emission computed tomographs for animal study. *IEEE Trans Nucl Sci* NS-32: 818-821, 1985

68. Tomitani T, Nohara N, Morayama H, et al: Development of a high resolution positron CT for animal studies. *IEEE Trans Nucl Sci* NS-32: 822-825, 1985

69. Computer Technology and Imaging, Inc. Knoxville, Tennessee, MODEL PT 931 ECAT Scanner System Description.

70. Derenzo SE, Huesman RH, Budinger FT, Cahoon JL, and Vuletich T: High resolution positron emission tomography using 3 mm wide bismuth germanate crystals. (in preparation) 1985

71. Karp JS and Muehllehner G: Performance of a position-sensitive scintillation detector. *Phys Med Biol* 1985 (in press)

72. Muehllehner G and Karp JS: A positron camera using position sensitive detectors: PENN–PET. (submitted for publication) 1985

This report was done with support from the Department of Energy. Any conclusions or opinions expressed in this report represent solely those of the author(s) and not necessarily those of The Regents of the University of California, the Lawrence Berkeley Laboratory or the Department of Energy.

Reference to a company or product name does not imply approval or recommendation of the product by the University of California or the U.S. Department of Energy to the exclusion of others that may be suitable.

TECHNICAL INFORMATION DEPARTMENT
LAWRENCE BERKELEY LABORATORY
UNIVERSITY OF CALIFORNIA
BERKELEY, CALIFORNIA 94720